**Carlos Vázquez**
Department of Applied Physics and Electronics,
Umeå University,
Umeå SE-901 87, Sweden
e-mail: carlos.vazquez@umu.se

**Leonid Fridman**
Professor
Department of Control Engineering and Robotics,
Universidad Nacional Autónoma de México,
Mexico City 04510, Mexico
e-mail: lfridman@unam.mx

**Joaquin Collado**
Professor
Department of Automatic Control CINVESTAV,
Av. IPN 2508,
Mexico City 07360, Mexico
e-mail: jcollado@ctrl.cinvestav.mx

**Ismael Castillo**
Department of Control Engineering and Robotics,
Universidad Nacional Autónoma de México,
Mexico City 04510, Mexico
e-mail: casism@gmail.com

# Second-Order Sliding Mode Control of a Perturbed-Crane

*A five degrees-of-freedom overhead crane system affected by external perturbations is the topic of study. Existing methods just handle the unperturbed case or, in addition, the analysis is limited to three or two degrees-of-freedom. A wide range of processes cannot be restricted to these scenarios and this paper goes a step forward proposing a control solution for a five degrees-of-freedom system under the presence of matched and unmatched disturbances. The contribution includes a model description and a second-order sliding mode (SOSM) control design ensuring the precise trajectory tracking for the actuated variables and at the same time the regulation of the unactuated variables. Furthermore, the proposed approach is supported by the design of strong Lyapunov functions providing an estimation of the convergence time. Simulations and experiments, including a comparison with a proportional-integral-derivative (PID) controller, verified the advantages of the methodology.* [DOI: 10.1115/1.4030253]

## 1 Introduction

The maneuvering with overhead crane systems has become the main part in many industrial activities where the efficiency in the cargo transportation process is crucial. This has motivated an intensive research on modeling and control during last decades. An important summary can be found in Ref. [1] and recent developments in Refs. [2–6]. Crane systems exhibit a complex behavior, with a nonlinear interaction between the trolley and the payload, where the acceleration of the trolley induces undesirable oscillations in the payload. In addition, uncertainties and external perturbations occur during regular operation conditions, degrading the overall control performance and increasing the risk of damages and accidents, see Refs. [2,5,6].

**1.1 State of the Art.** The solution to this problem remains still open and several attempts have been considered in the literature. When measurements are not available, input-shaping has proven to be useful for payload attenuation, as is shown in Ref. [7] for the case of a two-dimensional overhead crane and in Ref. [8] for the case of a tower crane; as well its application for the transient sway, as in Ref. [9], the skew control in Refs. [10] and [11] for the residual sway suppression considering damping. In Ref. [12], the passivity properties of the crane permit the design of feedback control laws using only the measurements of the trolley position for a two-dimensional overhead crane with constant cable length. Some methods to measure the payload oscillations have been proposed in Refs. [13–16], opening new possibilities to include the payload oscillation measurements in real environments. Using the measurement of the payload oscillations a nonlinear scheme has been proposed in Ref. [17] for the case of a three-dimensional (3D) overhead crane with constant cable length. Considering the measurements of angular and linear displacement a three degrees-of-freedom overhead crane is studied in Ref. [4] neglecting unmatched perturbations in the analysis. Mostly, trajectory planning strategies have been proposed in Ref. [18]. A partial feedback linearization approach was presented in Refs. [19,20] for the case of varying cable length. In all mentioned approaches, unmatched perturbations were not taking into account in the control design and cannot be handled by the proposed controllers. In addition, when velocity estimation is required the use of dirty time derivatives is a common practice.

**1.2 Methodology.** The design of control laws under the presence of heavy uncertainty conditions is one of the main problems of modern control theory. In this scenario, the SM methodology offers very good robustness/insensitivity properties again a wide variety of external disturbances as well as model uncertainties, see Ref. [21]. The main disadvantage of the SM controllers is the so-called *chattering effect*, a high frequency commutation in the control signal. This discontinuous input of high frequency is not suitable for the majority of the actuators. For this purpose, high-order SMs (HOSM) have proven to reduce the *chattering effect* without compromising the SM robustness/insensitivity properties, see Refs. [22–25].

In particular, for the overhead crane system, SOSM control techniques have been considered in Refs. [26,27]. A SM antisway control of an offshore container crane is proposed in Ref. [28]. In Ref. [29], an adaptable scheme is presented. The actuator fault diagnosis problem for a 3D overhead crane was studied in Ref. [30] using HOSM differentiators. However, when unmatched perturbations are present, the appropriate SM enforcement is an open challenge, see Ref. [24]. In order to deal with unmatched perturbations two directions have been taken: the minimization of unmatched perturbations in combination with robust schemes, see Ref. [31] and the compensation via observer and sliding-surface design, see Refs. [32–34]. Considering time-varying linear models the parametric resonance case was studied in Refs. [5,6].

**1.3 Contribution.** This paper presents the modeling and control design for a five degrees-of-freedom overhead crane system under the presence of matched and unmatched perturbations. The approach uses the twisting and super-twisting (ST) algorithms, together with the appropriate design of the sliding surface.

Contributed by the Dynamic Systems Division of ASME for publication in the Journal of Dynamic Systems, Measurement, and Control. Manuscript received October 10, 2014; final manuscript received March 24, 2015; published online April 24, 2015. Assoc. Editor: Hashem Ashrafiuon.

The trolley and payload angular positions are assumed to be available for measurement and their corresponding time derivatives are obtained via SOSM differentiators. With this aim, a nonconventional partial feedback linearization approach, allowing the inclusion of uncertainties and external perturbations is proposed. Then, the design of a sliding manifold based on virtual holonomic constraints, guaranteeing the stability of the zero dynamics under the presence of unmatched perturbations is presented. Finally, a SOSM control design is proposed. There are crucial differences with respect other works which are summarized below:

- First, model uncertainties as well as matched and unmatched perturbations are introduced in the modeling and control design for a five degrees-of-freedom perturbed-crane.
- A nonconventional partial feedback linearization approach is proposed, allowing the inclusion of external perturbations as well as the SM enforcement via twisting and ST algorithms.
- A new Lyapunov function for twisting algorithm is presented providing an estimation of convergence time and recovering Levant's inequalities.
- Large perturbations and disturbances are introduced in simulations and experiments which include a large initial swing angle and angular velocity, uncertainties in the parameters, a gust wind perturbation, and a friction force.
- A comparison with a PID algorithm is presented.

The structure of the paper is organized as follows: In Sec. 2, the mathematical model is described. Section 3 presents the SOSM control design. Simulations are presented in Sec. 4. The experimental results performed with a laboratory crane are presented in Sec. 5. Finally in Sec. 6, the conclusions are drawn for this study.

## 2 Mathematical Model

In this section, the mathematical model of a 3D overhead crane system, in the presence of external disturbances is presented. The test bench is a laboratory Inteco crane, shown in Fig. 1, and following [35] the corresponding coordinate system is described in Fig. 2. The payload is considered as a point mass and the mass and stiffness of the cable are neglected. The following notation is used: $m_c$ is the trolley mass, $m_r$ the rail mass, $m_p$ the payload mass, and $l$ is the length of the hoisting cable. The control problem is tracking for the actuated variables $x$, $y$, and $l$, and regulation for the unactuated variables $\theta_x$ and $\beta$, in the presence of the external perturbations $\mathbf{d}_1(t)$ and $\mathbf{d}_2(t)$.

**2.1 Modeling.** The position of the load in the fixed coordinate system is $(x_p, y_p, z_p) = (x + l\sin\theta_x\cos\beta, y + l\sin\beta, -l\cos\beta\cos\theta_x)$, where $x$, $y$, $l$, $\theta_x$, and $\beta$ are defined as the generalized coordinates that describe the motion. The model of the overhead crane can be obtained applying the Euler–Lagrange

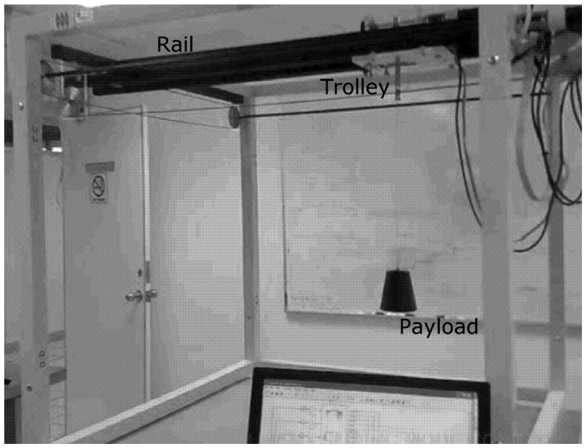


**Fig. 1 Inteco 3D-crane**

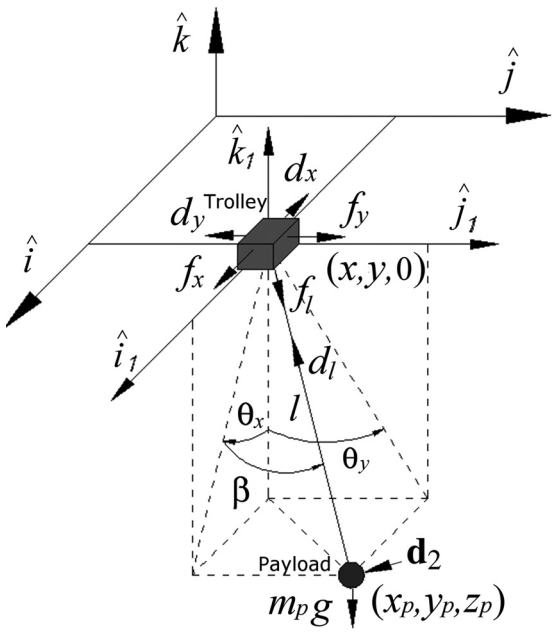


**Fig. 2 Coordinate system**

equation, see Ref. [35]. The corresponding Lagrangian is given by $\mathscr{L} = T - m_p g l(1 - \cos\theta_x\cos\beta)$, with $T = (1/2)m_p(\dot{x}_p^2 + \dot{y}_p^2 + \dot{z}_p^2) + (1/2)(m_x\dot{x}^2 + m_y\dot{y}^2 + m_p\dot{z}^2)$, where $m_x = m_p + m_c + m_r$ and $m_y = m_p + m_c$. The next step is to apply the Euler–Lagrange equation, obtaining the expression below:

$$\begin{aligned} \mathbf{M}_{11}\ddot{\mathbf{q}}_1 + \mathbf{M}_{12}\ddot{\mathbf{q}}_2 + \mathbf{h}_1 + \boldsymbol{\phi}_1 &= \mathbf{f} + \mathbf{d}_1, \\ \mathbf{M}_{21}\ddot{\mathbf{q}}_1 + \mathbf{M}_{22}\ddot{\mathbf{q}}_2 + \mathbf{h}_2 + \boldsymbol{\phi}_2 &= \mathbf{d}_2 \end{aligned} \tag{1}$$

where the related terms are $\mathbf{q}_1 = [x, y, l]^{\mathrm{T}}, \mathbf{q}_2 = [\theta_x, \beta]^{\mathrm{T}}$, $\mathbf{f} = \begin{bmatrix} f_x \\ f_y \\ f_z \end{bmatrix}$, $\mathbf{M}_{11} = \begin{bmatrix} m_x & 0 & m_p\sin\theta_x\cos\beta \\ 0 & m_y & m_p\sin\beta \\ m_p\sin\theta_x\cos\beta & m_p\sin\beta & m_p \end{bmatrix}$, $\mathbf{M}_{12} = \begin{bmatrix} m_p l\cos\theta_x\cos\beta & -m_p l\sin\theta_x\sin\beta \\ 0 & m_p l\cos\beta \\ 0 & 0 \end{bmatrix}$, $\mathbf{M}_{22} = \begin{bmatrix} m_p l^2\cos^2\beta & 0 \\ 0 & m_p l^2 \end{bmatrix}$ and $\mathbf{M}_{21} = \begin{bmatrix} m_p l\cos\theta_x\cos\beta & 0 & 0 \\ -m_p l\sin\theta_x\sin\beta & m_p l\cos\beta & 0 \end{bmatrix}$. The Coriolis and centrifugal terms: $\mathbf{h}_1 = [h_{11}, -m_p l\sin\beta\dot{\beta}^2 + 2m_p\cos\beta\dot{l}\dot{\beta}, -m_p l\cos^2\beta\dot{\theta}_x^2 - m_p l\dot{\beta}^2]^{\mathrm{T}}$, $\mathbf{h}_2 = \begin{bmatrix} 2m_p\dot{l}\dot{\theta}_x\cos^2\beta - 2m_p l^2\cos\beta\sin\beta\dot{\theta}_x\dot{\beta} \\ 2m_p\dot{l}\dot{\beta} + m_p l^2\cos\beta\sin\beta\dot{\theta}_x^2 \end{bmatrix}$, where $h_{11} = -m_p l\sin\theta_x\cos\beta(\dot{\theta}_x^2 + \dot{\beta}^2) - 2m_p\sin\theta_x\sin\beta\dot{l}\dot{\beta} + 2m_p\cos\theta_x\cos\beta\dot{l}\dot{\theta}_x - 2m_p l\cos\theta_x\sin\beta\dot{\theta}_x\dot{\beta}$. The gravitational terms $\boldsymbol{\phi}_1$ and $\boldsymbol{\phi}_2$ are $\boldsymbol{\phi}_1 = [0, 0, \phi_l]^{\mathrm{T}}, \boldsymbol{\phi}_2 = [m_p l g\cos\beta\sin\theta_x m_p l g\cos\theta_x\sin\beta]^{\mathrm{T}}$, where $\phi_l = -m_p g\cos\beta\cos\theta_x$. The terms $\mathbf{d}_1(t) = [d_x, d_y, d_l]^{\mathrm{T}}$ and $\mathbf{d}_2(t) = [d_{\theta_x}, d_\beta]^{\mathrm{T}}$ represents the matched and unmatched external perturbations, respectively.

**2.2 Partial Feedback Linearization With the Inclusion of Perturbations.** System (1) can be rewritten as it is shown below

$$\begin{aligned} \mathbf{M}\ddot{\mathbf{q}}_1 + \mathbf{h} + \boldsymbol{\phi} + \boldsymbol{\phi}_1 &= \mathbf{f} + \mathbf{d}_0, \\ \mathbf{M}_{22}\ddot{\mathbf{q}}_2 + \mathbf{h}_2 + \boldsymbol{\phi}_2 &= -\mathbf{M}_{21}\ddot{\mathbf{q}}_1 + \mathbf{d}_2 \end{aligned}$$

where $\boldsymbol{\phi} = -\mathbf{M}_{12}\mathbf{M}_{22}^{-1}\boldsymbol{\phi}_2$, $\mathbf{M} = \mathbf{M}_{11} - \mathbf{M}_{12}\mathbf{M}_{22}^{-1}\mathbf{M}_{21}$, $\mathbf{h} = \mathbf{h}_1 - \mathbf{M}_{12}\mathbf{M}_{22}^{-1}\mathbf{h}_2$, $\mathbf{d}_0 = \mathbf{d}_1 - \mathbf{M}_{12}\mathbf{M}_{22}^{-1}\mathbf{d}_2 = [\bar{d}_x, \bar{d}_y, d_l]^{\mathrm{T}}$, with: $\bar{d}_x = d_x - (\cos\theta_x/l\cos\beta)d_{\theta_x} + (1/l)\sin\theta_x\sin\beta d_\beta$ and $\bar{d}_y = d_y - (1/l)\cos\beta d_\beta$. The term $\boldsymbol{\phi}_1$ is considered as an unknown term, as well as the

external perturbations $\mathbf{d}_0$ and $\mathbf{d}_2$, nevertheless all of them are bounded. Setting $\mathbf{u}=[\mathbf{u}_0,u_l],\mathbf{u}_0\in\mathbb{R}^2,u_l\in\mathbb{R}$ and following the partial feedback linearization proposed in Ref. [36], it is defined:

$$\mathbf{f}=\mathbf{h}+\boldsymbol{\phi}+\mathbf{M}\mathbf{u} \tag{2}$$

obtaining

$$\begin{aligned}\ddot{\mathbf{q}}_1&=\mathbf{u}+\mathbf{M}^{-1}(\mathbf{d}_0-\boldsymbol{\phi}_1),\\ \mathbf{M}_{22}\ddot{\mathbf{q}}_2+\mathbf{h}_2+\boldsymbol{\phi}_2&=-\mathbf{M}_{21}\mathbf{u}+\bar{\mathbf{d}}_2\end{aligned} \tag{3}$$

where $\bar{\mathbf{d}}_2=\mathbf{d}_2-\mathbf{M}_{21}\mathbf{M}^{-1}(\mathbf{d}_0-\boldsymbol{\phi}_1)$. In this case $\mathbf{M}^{-1}(\mathbf{d}_0-\boldsymbol{\phi}_1)=[\bar{\mathbf{d}}_1,\bar{d}_l]^{\mathrm{T}}$, with $\bar{\mathbf{d}}_1=[((d_l-\phi_l)\cos\beta\sin\theta_x+\bar{d}_x)/(m_p-m_x),((d_l-\phi_l)\sin\beta+\bar{d}_y)/(m_p-m_y)]^{\mathrm{T}}$ and $\bar{d}_l=\bar{d}_y m_p\sin\beta+\bar{d}_x m_p\cos\beta\sin\theta_x-m_0(d_l-\phi_l)/m_p(m_p-m_x)(m_p-m_y)$, with $m_0=m_p m_y\sin^2\theta_x\sin^2\beta-(m_y-m_p\cos^2\beta)(m_x-m_p\cos^2\theta_x)$. Taking into account that the last column of $\mathbf{M}_{21}$ is a zero vector, system (3) can be written as

$$\ddot{\mathbf{q}}_{10}=\mathbf{u}_0+\bar{\mathbf{d}}_1 \tag{4}$$

$$\ddot{l}=u_l+\bar{d}_l \tag{5}$$

$$\mathbf{M}_{22}\ddot{\mathbf{q}}_2+\mathbf{h}_2+\boldsymbol{\phi}_2=-\overline{\mathbf{M}}_{21}\ddot{\mathbf{q}}_{10}+\bar{\mathbf{d}}_2 \tag{6}$$

$\ddot{\mathbf{q}}_{10}=[\ddot{x},\ddot{y}]^{\mathrm{T}},\overline{\mathbf{M}}_{21}=\begin{bmatrix}m_p l\cos\theta_x\cos\beta & 0\\ -m_p l\sin\theta_x\sin\beta & m_p l\cos\beta\end{bmatrix}$. In conclusion, a system formed by the dynamics (4)–(6) is obtained. The cable length dynamic, (5), are decoupled and affected by the perturbation $\bar{d}_l$. The dynamics of the trolley, subsystem (4), are affected by the perturbation $\bar{\mathbf{d}}_1$. The unactuated dynamics, payload oscillation, are given by Eq. (6) and affected by the vanishing uncoupled perturbation $\bar{\mathbf{d}}_2$ and the Coriolis and gravity terms, $\mathbf{h}_2$ and $\boldsymbol{\phi}_2$, respectively.

**2.3 Model Simplification.** Overhead crane systems have a restricted workspace, allowing us to introduce the next assumption:

($a_1$) For an overhead crane, the work space is defined in the domain $D=\{\mathbf{q}_2:\ \|\mathbf{q}_2\|_\infty<\pi/2\}$, which implies that there exists $\mathbf{M}_{22}^{-1}$ and $\overline{\mathbf{M}}_{21}^{-1}$. For practical purposes, it is considered $\|\mathbf{q}_2\|_\infty\le\pi/4$ which imply $\cos(\alpha)\approx 1$ and $\sin(\alpha)\approx\alpha$ for $\alpha=\theta_x,\beta$ in Eq. (6).

In the considered domain, expression (6) has the next form

$$\ddot{\mathbf{q}}_2+2\frac{\dot{l}(t)}{l(t)}\dot{\mathbf{q}}_2+\frac{g}{l(t)}\mathbf{q}_2=-\frac{1}{l(t)}\ddot{\mathbf{q}}_{10}+\frac{1}{m_p l^2(t)}\bar{\mathbf{d}}_2 \tag{7}$$

In Eq. (7), the logarithmic derivative of $l$, $\dot{l}/l$, appears as a time varying damping. In order to avoid this term, it is convenient to define the new coordinate $\mathbf{q}_{20}=l(t)\mathbf{q}_2$ (angular momentum), which results in the next representation

$$\ddot{\mathbf{q}}_{20}+\frac{1}{l(t)}(g-\ddot{l}(t))\mathbf{q}_{20}=-\mathbf{u}_0-\bar{\mathbf{d}}_1+\frac{1}{m_p l(t)}\bar{\mathbf{d}}_2 \tag{8}$$

Note that the terms related with $\dot{\mathbf{q}}_{20}$ are canceled in Eq. (8). For maneuvering operations, it is necessary to specify the desired trajectories; for this purpose, it is possible to define the cable length, $l$, as a time varying parameter, satisfying the next properties: $l(t)=l_0(1+\varepsilon r(t))$ and $0<\underline{l}<l(t)<\bar{l}$, where $l_0=(\underline{l}+\bar{l})/2$ and $\varepsilon|r(t)|<1$. In addition: $1/l(t)=1/l_0(1+l_\varepsilon(t))$, where $l_\varepsilon(t)=\sum_{i=1}^{\infty}(-1)^i(\varepsilon r(t))^i$ and $|l_\varepsilon|\le(\varepsilon/1-\varepsilon)=\varepsilon_l$, see Ref. [6]. Substituting $1/l(t)$ in Eq. (8)

$$\ddot{\mathbf{q}}_{20}+(\omega_0^2+\lambda_0(t))\mathbf{q}_{20}=-\mathbf{u}_0-\bar{\mathbf{d}}_1+\lambda_1(t)\bar{\mathbf{d}}_2 \tag{9}$$

where $\omega_0^2=(g/l_0),\lambda_0(t)=-(1/l_0)(\ddot{l}+(\ddot{l}-g)l_\varepsilon)$ and $\lambda_1(t)=(1/m_p l(t))$. In summary, after applying the partial feedback linearization approach, it is obtained the system dynamics (4), (5), and (9), valid in the domain $D$. The control problems of tracking and regulation will be studied in Sec. 3, proposing the appropriate design of a sliding manifold.

## 3 SOSM Control Design

First, the tracking errors, $\mathbf{e}$ and $e_l$ are defined $e_l=l-l_{\mathrm{ref}}$, $\mathbf{e}=\mathbf{q}_{10}-\mathbf{q}_{\mathrm{ref}}$, where $\mathbf{q}_{\mathrm{ref}}=[x_{\mathrm{ref}},y_{\mathrm{ref}}]^{\mathrm{T}}$ and vector $\mathbf{e}$ represents the error of the trolley position in its two components $(x,\ y)$, obtaining the error dynamics

$$\ddot{e}_l=u_l+\bar{d}_l-\ddot{l}_{\mathrm{ref}} \tag{10}$$

$$\ddot{\mathbf{e}}=\mathbf{u}_0+\bar{\mathbf{d}}_1-\ddot{\mathbf{q}}_{\mathrm{ref}} \tag{11}$$

It is convenient to define the state space representations for dynamics (9)–(11). Note that Eq. (10) is decoupled with the state space representation given below:

$$\underbrace{\begin{bmatrix}\dot{e}_l\\ \ddot{e}_l\end{bmatrix}}_{\dot{\mathbf{e}}_l}=\begin{bmatrix}0&1\\0&0\end{bmatrix}\underbrace{\begin{bmatrix}e_l\\ \dot{e}_l\end{bmatrix}}_{\mathbf{e}_l}+\begin{bmatrix}0\\1\end{bmatrix}(u_l+\bar{d}_l-\ddot{l}_{\mathrm{ref}}) \tag{12}$$

On the other hand, dynamics (9) and (11) are coupled sharing the same control input $\mathbf{u}_0$ as well as the matched perturbation $\bar{\mathbf{d}}_1$. The state space representation for Eqs. (9) and (11) is given below:

$$\underbrace{\begin{bmatrix}\dot{\mathbf{e}}\\ \ddot{\mathbf{e}}\\ \dot{\mathbf{q}}_{20}\\ \ddot{\mathbf{q}}_{20}\end{bmatrix}}_{\dot{\mathbf{q}}}=\bar{\mathbf{A}}\underbrace{\begin{bmatrix}\mathbf{e}\\ \dot{\mathbf{e}}\\ \mathbf{q}_{20}\\ \dot{\mathbf{q}}_{20}\end{bmatrix}}_{\mathbf{q}}+\mathbf{b}_0(\mathbf{u}_0+\bar{\mathbf{d}}_1)+\mathbf{b}_1\ddot{\mathbf{q}}_{\mathrm{ref}}+\lambda_1\mathbf{b}_2\bar{\mathbf{d}}_2 \tag{13}$$

where $\mathbf{b}_0=[\mathbf{0},\ \mathbf{I}_{2\times2},\ \mathbf{0},\ -\mathbf{I}_{2\times2}]^{\mathrm{T}}$, $\bar{\mathbf{A}}=\mathbf{A}_0+\Delta\mathbf{A}$, with $\mathbf{A}_0=\begin{bmatrix}\mathbf{0}&\mathbf{I}_{2\times2}&\mathbf{0}&\mathbf{0}\\ \mathbf{0}&\mathbf{0}&\mathbf{0}&\mathbf{0}\\ \mathbf{0}&\mathbf{0}&\mathbf{0}&\mathbf{I}_{2\times2}\\ \mathbf{0}&\mathbf{0}&-\omega_0^2\mathbf{I}_{2\times2}&\mathbf{0}\end{bmatrix}$, $\Delta\mathbf{A}=\begin{bmatrix}\mathbf{0}&\mathbf{0}&\mathbf{0}&\mathbf{0}\\ \mathbf{0}&\mathbf{0}&\mathbf{0}&\mathbf{0}\\ \mathbf{0}&\mathbf{0}&\mathbf{0}&\mathbf{0}\\ \mathbf{0}&\mathbf{0}&\lambda_0(t)\mathbf{I}_{2\times2}&\mathbf{0}\end{bmatrix}$, $\mathbf{b}_1=[\mathbf{0},\ -\mathbf{I}_{2\times2},\ \mathbf{0},\ \mathbf{0}]^{\mathrm{T}}$ and $\mathbf{b}_2=[\mathbf{0},\ \mathbf{0},\ \mathbf{0},\ \mathbf{I}_{2\times2}]^{\mathrm{T}}$. Now, consider the sliding outputs

$$\begin{aligned}\sigma_l&=e_l,\\ \sigma_q&=\psi_1(\mathbf{e},\dot{\mathbf{e}})-\psi_2(\mathbf{q}_{20},\dot{\mathbf{q}}_{20})\end{aligned} \tag{14}$$

where $\psi_1(\cdot)=\mathbf{C}_3\dot{\mathbf{e}}+\mathbf{C}_2\mathbf{e}+\mathbf{C}_1\int_0^t\mathbf{e}(\tau)d\tau$, and $\psi_2(\cdot)=\mathbf{C}_6\dot{\mathbf{q}}_{20}+\mathbf{C}_5\mathbf{q}_{20}+\mathbf{C}_4\int_0^t\mathbf{q}_{20}(\tau)d\tau$. Note that $\sigma_l$ has relative degree 2 and $\boldsymbol{\sigma}_q=[\sigma_x,\sigma_y]^{\mathrm{T}}$ has relative degree 1. The parameters $\mathbf{C}_i$, $i=1,...,6$, are $2\times2$ diagonal matrices of positive gains. Taking the first derivative of $\boldsymbol{\sigma}_q$ and the second time derivative of $\sigma_l$

$$\ddot{\sigma}_l=u_1+\bar{d}_l-\ddot{l}_{\mathrm{ref}} \tag{15}$$

$$\dot{\boldsymbol{\sigma}}_q=(\mathbf{C}_3+\mathbf{C}_6)\mathbf{u}_0+\mathbf{K}\mathbf{q}_2+\mathbf{d}_q \tag{16}$$

where $\mathbf{d}_q=(\mathbf{C}_3+\mathbf{C}_6)\bar{\mathbf{d}}_1+\mathbf{d}_3$ with $\mathbf{d}_3=-\mathbf{C}_3\ddot{\mathbf{q}}_{\mathrm{ref}}-\lambda_1(t)\mathbf{C}_6\bar{\mathbf{d}}_2-\mathbf{C}_6(\omega_0^2+\lambda_0(t))\mathbf{q}_{20}$. The matrix $\mathbf{K}$ is given next $\mathbf{K}=[\mathbf{C}_1,\mathbf{C}_2,-\mathbf{C}_4,-\mathbf{C}_5]$.

*Remark 1.* Choosing convenient trajectories $\ddot{\mathbf{q}}_{\mathrm{ref}}$ and $\ddot{l}_{\mathrm{ref}}$, with Lipschitz continuous second time derivative, the perturbations satisfy the following bounds $|\bar{d}_l|\le L_l$, $\|\mathbf{d}_q\|\le L_0$ and $\|\dot{\mathbf{d}}_q\|\le L_1$.

From the invariance conditions $\ddot{\sigma}_l = \dot{\sigma}_1 = \sigma_l = 0$ and $\dot{\boldsymbol{\sigma}}_q = \boldsymbol{\sigma}_q = 0$, the equivalent control is obtained: $\mathbf{u}_{\text{eq}} = [-\bar{d}_l + \ddot{l}_{\text{ref}}, -\bar{\mathbf{d}}_1 + (\mathbf{C}_3 + \mathbf{C}_6)^{-1}(-\mathbf{K}\mathbf{q}_2 - \mathbf{d}_3)]^{\text{T}}$. In the sliding manifold, the virtual holonomic constraints $\psi_1(\cdot) = \psi_2(\cdot)$ and $e_l = 0$ are imposed.

**3.1 Stability Analysis of Zero Dynamics.** With the equivalent control arise the corresponding zero dynamics

$$\dot{\mathbf{e}}_l = \mathbf{e}_l = \mathbf{0} \tag{17}$$

$$\dot{\mathbf{q}} = (\mathbf{A}_0 - \mathbf{b}\mathbf{K})\mathbf{q} + \mathbf{d}(\mathbf{q}_2, t) \tag{18}$$

where $\mathbf{b} = \mathbf{b}_0(\mathbf{C}_3 + \mathbf{C}_6)^{-1}$. Stability of Eq. (17) is trivial since variable $l$ is completely actuated and decoupled. This is not the case of Eq. (18) where unactuated variables are present as well as unmatched perturbations. From Eq. (18), it is evident that the equivalent control compensates exactly the matched perturbation $\bar{\mathbf{d}}_1$, and induces the stabilizing term $-\mathbf{K}\mathbf{q}_2$; however the unmatched perturbation $\mathbf{d}(\mathbf{q}_2, t) = \Delta\mathbf{A}\mathbf{q}_2 + \mathbf{b}_0(\mathbf{C}_3 + \mathbf{C}_6)^{-1}\mathbf{d}_3 + \mathbf{b}_1\ddot{\mathbf{q}}_{\text{ref}} + \lambda_1(t)\mathbf{b}_2\bar{\mathbf{d}}_2$ is still present. Furthermore, with the design of suitable trajectories for $\mathbf{q}_{\text{ref}}$ and $l_{\text{ref}}$, with Lipschitz continuous second time derivative, it is possible to consider the next additional assumption

$$(\text{a}_2) \qquad \|\mathbf{d}(\mathbf{q}_2, t)\| \leq \bar{\gamma}_1\|\mathbf{q}_2\| + \bar{\gamma}_0$$

Here $\bar{\gamma}_0$ and $\bar{\gamma}_1$ are positive constants. Now consider a quadratic Lyapunov function $V = (1/2)\mathbf{q}_2^{\text{T}}\mathbf{P}\mathbf{q}_2$ with $\mathbf{P} = \mathbf{P}^{\text{T}} > 0$. Taking the time derivative of $V$: $\dot{V} = (1/2)\mathbf{q}_2^{\text{T}}(\mathbf{A}^{\text{T}}\mathbf{P} + \mathbf{P}\mathbf{A})\mathbf{q}_2 + \mathbf{d}^{\text{T}}\mathbf{P}\mathbf{q}_2$, where $\mathbf{A} = \mathbf{A}_0 - \mathbf{b}\mathbf{K}$, and looking for a matrix $\mathbf{P}$ solution of the Lyapunov equation $\mathbf{A}^{\text{T}}\mathbf{P} + \mathbf{P}\mathbf{A} = -2\mathbf{I}$, we obtain: $\dot{V} \leq -\|\mathbf{q}_2\|^2 + \|\mathbf{d}\|\lambda_{\max}[\mathbf{P}]\|\mathbf{q}_2\|$, which implies the following result:

THEOREM 1. *The ultimate bounded stability of system (18) is guaranteed if the following condition is satisfied*:

$$\frac{\|\mathbf{d}(\mathbf{q}_2, t)\|}{\|\mathbf{q}_2\|} \leq \frac{1}{\lambda_{\max}[\mathbf{P}]} \tag{19}$$

*where* $\mathbf{d}(\mathbf{q}_2, t)$ *satisfy assumption* $(\text{a}_2)$ *and* $\mathbf{P}$ *is the solution of the Lyapunov equation*: $\mathbf{A}^{\text{T}}\mathbf{P} + \mathbf{P}\mathbf{A} = -2\mathbf{I}$, *with* $\mathbf{A} = \mathbf{A}_0 - \mathbf{b}\mathbf{K}$.

*Remark 2.* $\lambda_{\max(\min)}[\cdot]$ denotes the operation of taking the largest (smallest) eigenvalue of some symmetric matrix. The Euclidean norm of a vector $\zeta$ and the induced norm of a matrix $\mathbf{A}$ are denoted by $\|\zeta\|$ and $\|\mathbf{A}\|$, respectively.

Further details of this theorem can be found in Ref. [37], Sec. 13.9. In the case of $\bar{\gamma}_0 = 0$, condition (19) implies the exponential stability of the zero dynamics.

**3.2 SM Enforcement.** In this section, the SM enforcement design is introduced. Furthermore, the Lyapunov analysis for the twisting controller using a new nondifferentiable strong Lyapunov function, providing an estimation of the convergence time, is presented.

The SM enforcement of Eq. (16) can be achieved by the ST algorithm. For this purpose, the next control law is proposed

$$\mathbf{u}_0 = (\mathbf{C}_3 + \mathbf{C}_6)^{-1}(-\mathbf{K}\mathbf{q}_2 + \nu) \tag{20}$$

$$\nu = -\mathbf{K}_1\begin{bmatrix} |\sigma_x|^{\frac{1}{2}}\text{sign}(\sigma_x) \\ |\sigma_y|^{\frac{1}{2}}\text{sign}(\sigma_y) \end{bmatrix} - \mathbf{K}_2\int_0^t \begin{bmatrix} \text{sign}(\sigma_x) \\ \text{sign}(\sigma_y) \end{bmatrix} d\tau$$

The parameters $\mathbf{K}_1$ and $\mathbf{K}_2$ are $2 \times 2$ diagonal matrices of positive gains. A necessary condition of convergence for ST algorithm is $\lambda_{\min}[\mathbf{K}_2] > L_1$, if in addition, we select a $\lambda_{\min}[\mathbf{K}_1]$ sufficiently large, the controller $\mathbf{u}_0$ guarantee the appearance of a SOSM $\sigma_0 = \dot{\boldsymbol{\sigma}}_0 = 0$ in system (16). A very crude condition is $2(\lambda_{\min}[\mathbf{K}_2] + L_1)^2/(\lambda_{\min}[\mathbf{K}_1]^2(\lambda_{\min}[\mathbf{K}_2] - L_1)) < 1$. Recently, in Ref. [38] it was demonstrated that for any $c_0 > 0$, $c_0 = \lambda_{\min}[\mathbf{K}_2] - L_1$, and $\delta > 0$, there exists $\lambda$ such that $\sigma_i$, $i = x, y$, is reduced to zero in finite time less than $(\sigma_i(0)/c_0) + \delta$, if $\lambda_{\min}[\mathbf{K}_1] > \lambda$. The convergence time cannot be less than $\sigma_i(0)/c_0, i = x, y$.

On the other hand, the SM enforcement of Eq. (15) can be achieved by the twisting algorithm

$$u_1 = -r_1\text{sign}(\sigma_l) - r_2\text{sign}(\dot{\sigma}_l) \tag{21}$$

where $r_1$ and $r_2$ are positive constants. In particular, for the twisting algorithm, the convergence condition, stated by Levant, is $r_1 > r_2 + L_l$ and $r_2 > L_l$, see Ref. [22]; with this condition the SOSM $\ddot{\sigma}_l = \dot{\sigma}_l = \sigma_l = 0$ is achieved in finite time. Recently, in Refs. [39,40] we can find the design based on strict Lyapunov functions which provides an estimation of the convergence time. In Sec. 3.3, a new strong Lyapunov function is proposed. In comparison with Ref. [40], the new Lyapunov function provides a reduced number of inequalities in the analysis and it preserve the conditions stated by Levant.

**3.3 Convergence Time, Twisting Algorithm.** One of the most important features of the SM approach is a *finite-time* reaching phase. However the corresponding Lyapunov functions may be nonsmooth in this case, see Ref. [41] where recently a detailed survey is presented. First, setting $\sigma_1 = \sigma_l$ and $\dot{\sigma}_l = \sigma_2$, Eq. (15) can be rewritten as below:

$$\dot{\sigma}_1 = \sigma_2, \quad \dot{\sigma}_2 = u_l + \bar{d}_l \tag{22}$$

where $|\bar{d}_l| \leq L_l$. Consider the candidate Lyapunov function

$$V = V_0^2 + \gamma_1|\sigma_1|^{\frac{3}{2}}\sigma_2\text{sign}(\sigma_1) \tag{23}$$

where $V_0 = (1/2)\sigma_2^2 + r_1|\sigma_1|$ and $\gamma_1$ is a positive constant, $\gamma_1 > 0$. Taking the time derivative of Eq. (23) along Eq. (15)

$$\dot{V} = \underbrace{2V_0\dot{V}_0}_{\text{a.}} + \underbrace{\frac{3}{2}\gamma_1|\sigma_1|^{\frac{1}{2}}\sigma_2^2}_{\text{b.}} + \underbrace{\gamma_1|\sigma_1|^{\frac{3}{2}}(u_l + \bar{d}_l)\text{sign}(\sigma_1)}_{\text{c.}}$$

a. $$2V_0\dot{V}_0 = 2V_0(-r_2|\sigma_2| + \bar{d}_i\sigma_2) \leq 2(r_2 - L_l)|\sigma_2|V_0 \leq -(r_2 - L_l)|\sigma_2|^3 - 2(r_2 - L_l)r_1|\sigma_1|\|\sigma_2|$$

b. $\frac{3}{2}\gamma_1|\sigma_1|^{\frac{1}{2}}\sigma_2^2 \leq \gamma_1(\sigma_2^3 + |\sigma_1|^{\frac{3}{2}})$

c. $\gamma_1|\sigma_1|^{\frac{3}{2}}(\bar{u}_i + \bar{d}_i)\text{sign}(\sigma_1) \leq -\gamma_1 r|\sigma_1|^{\frac{3}{2}}$

with $r = r_1 - r_2 - L_l > 0$. Considering $\gamma_1 < \min\{r_2 - L_l, r\}$

$$\dot{V} \leq -\bar{r}(|\sigma_1|^{\frac{3}{2}} + |\sigma_2|^3) \tag{24}$$

where $\bar{r} = \min\{r_2 - L_l - \gamma_1, (r-1)\gamma_1\}$. On the other hand, defining $\xi_1 = |\sigma_1|^{1/2}\ \text{sign}(\sigma_1)$ and $\xi_2 = \sigma_2$, function $V$ can be rewritten as: $V = (1/4)\sigma_2^4 + |\sigma_1|\boldsymbol{\xi}^T\mathbf{P}_\xi\boldsymbol{\xi}$, where $\boldsymbol{\xi} = [\xi_1, \xi_2]^{\text{T}}$ and $\mathbf{P}_\xi = \begin{bmatrix} r_1^2 & \gamma_1/2 \\ \gamma_1/2 & r_1 \end{bmatrix}$. Taking into account $r_1 > \frac{1}{4^{\frac{1}{3}}}\gamma_1^{\frac{2}{3}}$, it implies $\mathbf{P}_\xi > 0$. Moreover, $\lambda_{\min}[\mathbf{P}_\xi]\|\boldsymbol{\xi}\|^2|\sigma_1| \leq V \leq \frac{1}{4}\sigma_2^4 + \lambda_{\max}[\mathbf{P}_\xi]\|\boldsymbol{\xi}\|^2|\sigma_1|$, where $\|\boldsymbol{\xi}\|^2 = |\sigma_1| + \sigma_2^2$. Considering the right-hand side of the previous inequality, we have $V \leq \bar{\gamma}(\sigma_2^4 + |\sigma_1|^2 + \|\boldsymbol{\xi}\|^4)$, with $\bar{\gamma} = \max\{\frac{1}{4}, \frac{1}{2}\lambda_{\max}[\mathbf{P}_\xi]\}$. Taking into account $\|\boldsymbol{\xi}\|^4 \leq 2(|\sigma_1|^2 + \sigma_2^4)$, the next condition is obtained: $V \leq 3\bar{\gamma}(|\sigma_2|^4 + |\sigma_1|^2)$. Finally using Jensen's inequality

$$V \leq 3\bar{\gamma}(|\sigma_2|^4 + |\sigma_1|^2) \leq 3\bar{\gamma}(|\sigma_2|^3 + |\sigma_1|^{\frac{3}{2}})^{\frac{4}{3}} \tag{25}$$

From Eqs. (24) and (25), it follows $\dot{V} \leq -(\bar{r}/(3\bar{\gamma})^{\frac{3}{4}})V^{\frac{3}{4}}$. We just have proved the following:

THEOREM 2. *Using twisting algorithm, and considering the next expressions*

$$r_1 > r_2 > L_l,\ r_1 > r_2 + L_l,\ r_1 > \tfrac{1}{4^{\frac{2}{3}}}\gamma_1^{\frac{2}{3}},$$
$$0 < \gamma_1 < \min\{r_2 - L_l, r\}$$

*with* $r = r_1 - r_2 - L_l$. *The point* $\bar{\sigma} = [\sigma_1, \sigma_2] = [0,0]^{\mathrm{T}}$ *of system (22) is globally exact finite time stable. Moreover, an upper bound,* $T_{\mathrm{reach}}$, *of the convergence time of a trajectory starting at* $\bar{\sigma}(0)$ *can be estimated by:* $T_{\mathrm{reach}} \leq (4/\gamma)V_1^{\frac{1}{4}}(\bar{\sigma}(0))$, *with* $\gamma = (\bar{r}/(3\bar{\gamma})^{\frac{3}{4}})$, *where* $\bar{r} = \max\{r_2 - L_l - \gamma_1, r - \gamma_1\}$ *and* $\bar{\gamma} = \max\{\frac{1}{4}, \frac{1}{2}\lambda_{\max}[\mathbf{P}_\xi]\}$ *with* $\mathbf{P}_\xi = \begin{bmatrix} r_1^2 & \frac{\gamma_1}{2} \\ \frac{\gamma_1}{2} & r_1 \end{bmatrix}$.

## 4 Simulations

Simulations were performed in MATLAB/SIMULINK™, using the Euler integration method with a sample time of 1 ms. The considered parameters are $m_p = 1$ kg, $m_c = 0.6$ kg, $m_r = 1$ kg, and $g = 9.81$ m/s$^2$; the initial conditions are: $x(0) = 0.045$ m, $\dot{x}(0) = 0$ m/s, $y(0) = 0.055$ m, $\dot{y}(0) = 0$ m/s, $l(0) = 0.55$ m, $\dot{l}(0) = 0$ m/s, $\theta_x(0) = 4$ deg, $\dot{\theta}_x(0) = 0.57$ deg/s, $\beta(0) = 3$ deg and $\dot{\beta}(0) = 1.14$ deg/s. The reference trajectory for the trolley position is $q_{\mathrm{ref}}(t) = [x_{\mathrm{ref}}, y_{\mathrm{ref}}]^{\mathrm{T}}$, with: $\alpha_{\mathrm{ref}}(t) = b_i + a_i \sin(\omega_x t + \phi_i)\alpha = x, y$, where $b_x = b_y = 0.25, a_x = a_y = 0.2$, $\omega_x = \omega_y = 0.5, \phi_x = (\pi/2)$ and $\phi_y = 0$. Besides, the reference for the rope length is given by $l_{\mathrm{ref}} = 0.55 + 0.2\sin(0.6t)$. The external perturbations, considered in the simulation, are described below:

- For perturbation $\mathbf{d}_1$, a friction model previously considered in Refs. [4,42] is used in simulation: $\mathbf{d}_1 = [d_x, d_y, d_l]^{\mathrm{T}}$ with $d_\alpha = -\mu_\alpha\dot{\alpha} - \rho_\alpha \tanh(\dot{\alpha})$, for $\alpha = x, y, l$, and $\mu_x = \mu_y = \mu_l = 4$ kg/s and $\rho_x = \rho_y = 2$ and $\rho_l = 10$.
- For perturbation $\mathbf{d}_2$, a gust wind model, usually considered in wind studies, see Refs. [3,43], is considered: $\mathbf{d}_2 = [d_{\theta_x}, d_\beta]^{\mathrm{T}}$ with

$$d_i = \begin{cases} 0, & t < t_a, \\ \dfrac{a_{\max}}{2}\dfrac{2\pi}{t_b}\sin\left(\dfrac{2\pi}{t_b}t - \dfrac{t_a}{t_b}\right), & t_a < t \leq t_a + t_b, \\ 0, & t > t_a + t_b \end{cases}$$

where $a_{\max} = 0.1$, $t_b = 2$, and $t_a = 3$.

The control design is composed of three elements: partial feedback linearization (2), twisting algorithm (21) for the length $l$, and ST algorithm (20) for the tracking of the trolley position and the attenuation of payload oscillations. In addition to the perturbations, a deviation of 20% in the values of $m_p$, $m_c$, and $m_r$ was included in the simulation. The proposed twisting control parameters are given next: $r_1 = 46$ and $r_2 = 25$. In this case $L_l = 12$ and choosing $\gamma_1 = 1.5$, Theorem 2 give us an estimation of the convergence time, $T_{\mathrm{reach}} \leq 147V_1^{\frac{1}{4}}(\bar{\boldsymbol{\sigma}}(0))$, ensuring the SM $\dot{\sigma}_l = \sigma_l = 0$. Besides, the proposed parameter for the ST controller are: $\mathbf{K}_2 = 0.5I_{2\times2}$ and $\mathbf{K}_1 = I_{2\times2}$. In this case $L_1 = 0.4$, which implies $\lambda_{\min}[\mathbf{K}_2] > L_1$. Then, with $\lambda_{\min}[\mathbf{K}_1]$ sufficiently large we ensured $\dot{\boldsymbol{\sigma}} = \boldsymbol{\sigma} = 0$ in finite time, see Ref. [38]. The sign function is approximated by $\mathrm{sign}(\sigma) \approx (\sigma/(|\sigma| + \varepsilon))$, with $\varepsilon = 10^{-4}$. The time derivatives were obtained with the HOSM differentiator introduced in Ref. [23].

In order to adjust the desired system response, the parameters of matrix $\mathbf{K}$ should be selected. In the simulation we used:

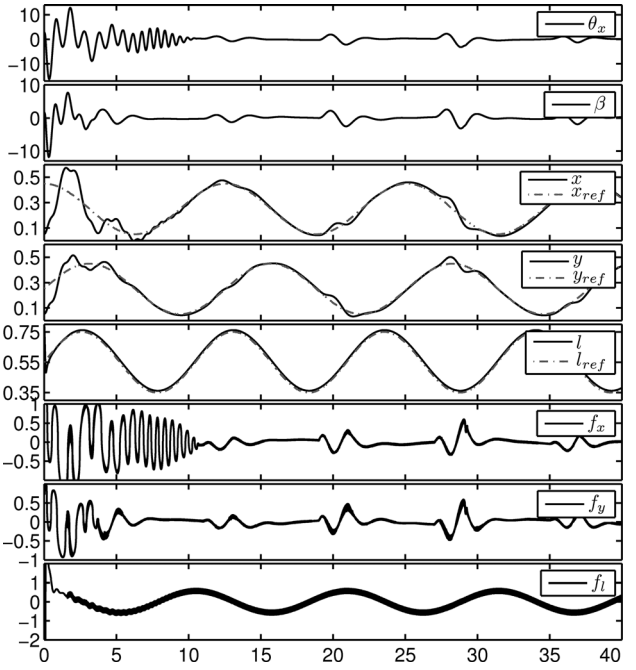


**Fig. 3 Simulation: trolley position and rope length (m), payload oscillations (deg), control actions (N) versus time (s)**

$\mathbf{C}_6 = 2I_{2\times2}$, $\mathbf{C}_5 = 12I_{2\times2}, \mathbf{C}_4 = 2I_{2\times2}$, $\mathbf{C}_3 = 2I_{2\times2}, \mathbf{C}_2 = 14I_{2\times2}$, $\mathbf{C}_1 = 4I_{2\times2}$. With this parameters, the eigenvalues of the matrix, $\mathbf{A}_0 - \mathbf{bK}$, are located at $\mathbf{E} = [-4.9887, -4.9887, -0.313, -0.313, -0.5991 \pm 3.3261i, -0.5991 \pm 3.3261i]$. Other parameters can be selected using pole place assignment or linear-quadratic-regulator (LQR) method. In our case the system parameters are given by $\mathbf{b}_0 = [\,\mathbf{0},\ \mathbf{I}_{2\times2},\ \mathbf{0},\ -\mathbf{I}_{2\times2}\,]^{\mathrm{T}}$, $\mathbf{A}_0$

$$= \begin{bmatrix} \mathbf{0} & \mathbf{I}_{2\times2} & \mathbf{0} & \mathbf{0} \\ \mathbf{0} & \mathbf{0} & \mathbf{0} & \mathbf{0} \\ \mathbf{0} & \mathbf{0} & \mathbf{0} & \mathbf{I}_{2\times2} \\ \mathbf{0} & \mathbf{0} & -\frac{9.81}{0.55}\mathbf{I}_{2\times2} & \mathbf{0} \end{bmatrix}$$

Defining the vector $\mathbf{E}$ containing the desired eigenvalues for the closed-loop system $\mathbf{A}_0 - \mathbf{b}_0\mathbf{K}$, the vector $\mathbf{K}$ can be obtained using the MATLAB command $\mathbf{K} = \mathrm{place}(\mathbf{A}_0, \mathbf{b}_0, \mathbf{E})$. On the other hand, defining appropriate matrices $\mathbf{Q} \in \mathbb{R}^{8\times8}, \mathbf{R} \in \mathbb{R}^{2\times2}$ and $\mathbf{N} \in \mathbb{R}^{8\times2}$ the MATLAB command $[\mathbf{K}, \mathbf{S}, \mathbf{E}] = \mathrm{lqr}(\mathbf{A}_0, \mathbf{b}_0, \mathbf{Q}, \mathbf{R}, \mathbf{N})$ can be used. A suggestion is given: $\mathbf{R} = \mathbf{I}_{2\times2}, \mathbf{N} = [-\mathbf{I}_{2\times2}, -\mathbf{I}_{2\times2}, \mathbf{0}, \mathbf{0}]^{\mathrm{T}}$ and $\mathbf{Q} = \mathrm{diag}([10\mathbf{I}_{2\times2}, 10\mathbf{I}_{2\times2}, 500\mathbf{I}_{2\times2}, 500\mathbf{I}_{2\times2}])$. In order to compare the performance of the SOSM differentiators [23], a comparison with an optimal spline approximation is presented. The spline approximation is an offline method, and it uses previous and future values of the measured position, see, e.g., Ref. 44. The smoothing spline is tuned in order to obtain the smoothest possible estimation and keeping the fitting error within the quantization interval. The simulation results are presented in Fig. 3. Figure 4 shows the time derivatives obtained (online) with the SOSM differentiator and the offline estimation.

## 5 Experiments

Experiments were performed on a laboratory Inteco™ 3D-crane. This crane is instrumented with high performance encoders for the measurement of the variables $(x, y, l, \theta_x, \beta)$, and they are interfaced to a personal computer with an Inteco™ data acquisition board. The control algorithms are implemented on MATLAB/SIMULINK™ environment. The estimation of the velocities $(\dot{x}, \dot{y}, \dot{l}, \dot{\theta}_x, \dot{\beta})$ are obtained with the HOSM differentiator proposed by Levant in Ref. [23]. In the experiment, we consider the same

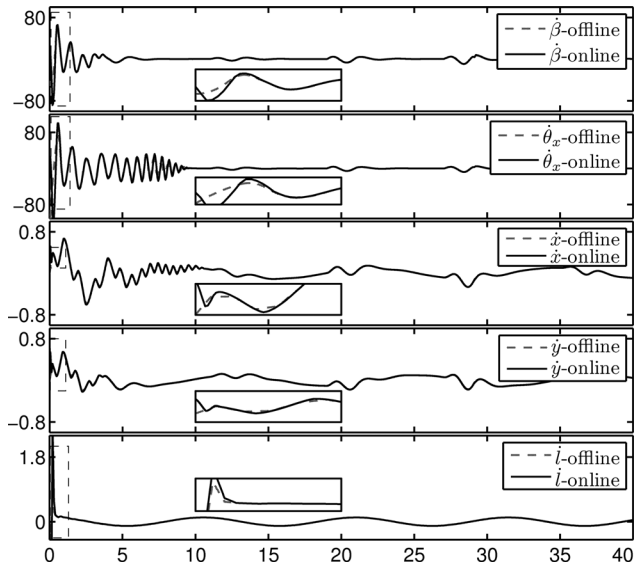


**Fig. 4 Velocity estimation: trolley and rope length (m/s) and payload oscillations (deg/s) versus time (s)**

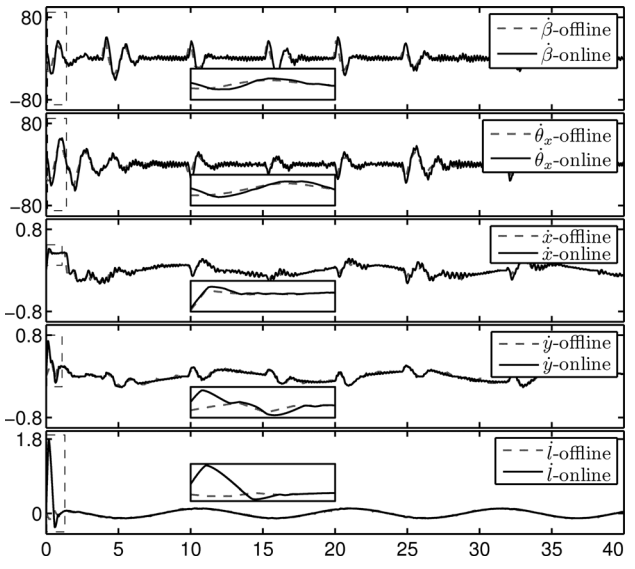


**Fig. 6 Velocity estimation: trolley and rope length (m/s) and payload oscillations (deg/s) versus time (s)**

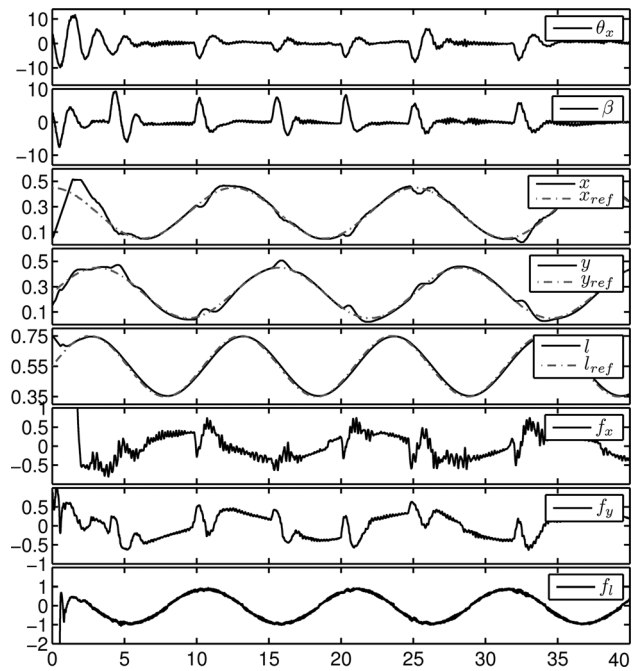


**Fig. 5 Experiment: trolley position and rope length (m), payload oscillations (deg), control actions (N) versus time (s)**

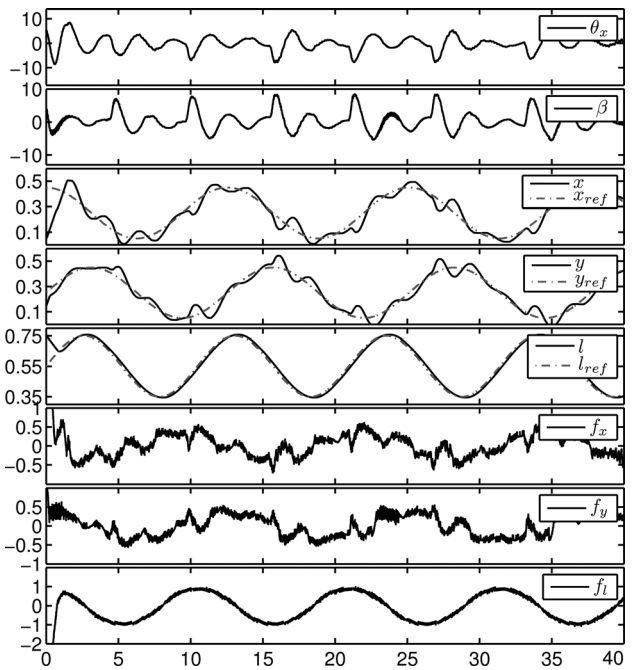


**Fig. 7 PID: trolley position and rope length (m), payload oscillations (deg), control actions (N) versus time (s)**

parameters as in simulation, with the exception of the perturbation $\mathbf{d}_2$, in the experiment the perturbation $\mathbf{d}_2$ consists of a sequence of several impacts over the payload, trying to simulate a gust wind disturbance during regular operation. Also, an initial payload swing was induced in the experiment.

The obtained results are presented in Fig. 5. Figure 6 shows the time derivatives obtained (online) with the SOSM differentiator and the offline estimation via splines, verifying a very good estimation of the velocities. Videos of experiments are available at[1].

*Remark 3*. The comparison of Fig. 3 versus Fig. 5 and Fig. 4 versus Fig. 6 shows how well resembles the experimentation versus simulations. Several sources of disturbances were introduced in the experiment presented in Fig. 5: Initial swing angle, gravity term $\phi_1$, uncertainty in the payload weight as well as matched and unmatched perturbations $\mathbf{d}_1$ and $\mathbf{d}_2$, respectively. Simulations and experiments verify the good performance of the proposed control law.

In addition, a comparison with the PID controller is presented. For comparison purposes, we implemented the PID control provided by Inteco™. This control law has the form: $f_\alpha = k_{p\alpha}e_\alpha + k_{d\alpha}\dot{e}_\alpha + k_{i\alpha}\int_0^t e_\alpha d\tau + k_\alpha\theta_\alpha$, where $e_\alpha$ represents the position error, for $\alpha = x, y$. Additionally, $f_l = k_{pl}e_l + k_{dl}\dot{e}_l + k_{il}\int_0^t e_l d\tau$. The considered parameters are: $k_{px} = k_{py} = k_{pl} = 10$, $k_{dx} = 2$, $k_{dy} = k_{dl} = 1$, $k_{ix} = 10$, $k_{iy} = 15$, $k_{il} = 20$, and $k_x = k_y = 10$. Since tuning rules are not well understood for underactuated mechanical systems, we adjust the parameters in order to obtain the best possible performance, increasing of this gains resulted in decreasing of

[1]https://sites.google.com/site/carlosvazquezcontact/videos

performance. Figure 7 shows the obtained results with the PID controller. From Fig. 7 is evident that the performance offered by the PID controller is not very good in order to achieve the tracking of the trolley and the attenuation of the payload oscillations under the presence of perturbations.

## 6 Conclusions

An overhead crane system affected by external perturbations is studied in the paper. The design of a SOSM controller, using twisting and ST algorithms is proposed in order to deal with model uncertainties and the external perturbations. An initial swing angle, uncertainties in the parameters, a gust wind perturbation and a friction force were successfully compensated with the proposed methodology. The performed simulations and experiments verified the expected performance for an overhead crane system. Additionally, a comparison with a PID controller is presented. Extensions for a large class of underactuated mechanical systems are considered for future work.

## References


[1] Abdel-Rahman, E. M., Nayfeh, A. H., and Masoud, Z. N., 2003, "Dynamics and Control of Cranes: A Review," J. Vib. Control, **9**(7), pp. 863–908.
[2] Ngo, Q. H., and Hong, K.-S., 2012, "Dynamics of the Container Crane on a Mobile Harbor," Ocean Eng., **53**, pp. 16–24.
[3] Tomczyk, J., Cink, J., and Kosucki, A., 2014, "Dynamics of an Overhead Crane Under a Wind Disturbance Condition," Autom. Constr., **42**, pp. 100–111.
[4] Sun, N., and Fang, Y., 2014, "Nonlinear Tracking Control of Underactuated Cranes With Load Transferring and Lowering: Theory and Experimentation," Automatica, **50**(9), pp. 2350–2357.
[5] Vázquez, C., Collado, J., and Fridman, L., 2014, "Super Twisting Control of a Parametrically Excited Overhead Crane," J. Franklin Inst., **351**(4), pp. 2283–2298.
[6] Vázquez, C., Collado, J., and Fridman, L., 2013, "Control of a Parametrically Excited Crane: A Vector Lyapunov Approach," IEEE Trans. Control Syst. Technol., **21**(6), pp. 2332–2340.
[7] Singhose, W., Porter, L., Keninson, M., and Kriikku, E., 2000, "Effects of Hoisting on the Input Shaping Control of Gantry Cranes," Control Eng. Pract., **8**(10), pp. 1159–1165.
[8] Blackburn, D., Lawrence, J., Danielson, J., Singhose, W., Kamoi, T., and Taura, A., 2010, "Radial-Motion Assisted Command Shapers for Nonlinear Tower Crane Rotational Slewing," Control Eng. Pract., **18**(5), pp. 523–531.
[9] Hong, K., Huh, C., and Hong, K.-S., 2003, "Command Shaping Control for Limiting the Transient Sway Angle of Crane Systems," Int. J. Control Autom. Syst., **1**(1), pp. 43–53.
[10] Ngo, Q., and Hong, K.-S., 2009, "Skew Control of a Quay Container Crane," J. Mech. Sci. Technol., **23**(12), pp. 3332–3339.
[11] Shah, U., and Hong, K.-S., 2014, "Input Shaping Control of a Nuclear Power Plants Fuel Transport System," Nonlinear Dyn., **77**(4), pp. 1737–1748.
[12] Fang, Y., Ma, B., Wang, P., and Zhang, X., 2012, "A Motion Planing-Based Adaptive Control Method for an Underactuated Crane System," IEEE Trans. Control Syst. Technol., **20**(1), pp. 241–248.
[13] Todd, M. D., Vohra, S. T., and Leban, F., 1997, "Dynamical Measurement of Ship Crane Load Pendulation," Proceedings of Oceans MTS/IEEE, pp. 1230–1236.
[14] Kim, Y.-S., Hong, K.-S., and Sul, S.-K., 2004, "Anti-Sway Control of Container Cranes: Inclinometer, Observer, and State Feedback," Int. J. Control Autom. and Syst., **2**(4), pp. 435–449.
[15] Schaub, H., 2008, "Rate-Based Ship-Mounted Crane Payload Pendulation Control System," Control Eng. Pract., **16**(1), pp. 132–145.
[16] Björkbom, M., Nethi, S., Eriksson, L. M., and Jäntti, R., 2011, "Wireless Control System Design and Co-Simulation," Control Eng. Pract., **19**(9), pp. 1075–1086.
[17] Chwa, D., 2011, "Nonlinear Tracking Control of 3-D Overhead Cranes Against the Initial Swing Angle and the Variation of Payload Weight," IEEE Trans. Control Syst. Technol., **17**(4), pp. 876–883.
[18] Lee, H.-H., 2005, "Motion Planning for the Three-Dimensional Overhead-Cranes With High-Speed Load Hoisting," Int. J. Control, **78**(12), pp. 875–886.
[19] Park, H., Chwa, D., and Hong, K.-S., 2007, "A Feedback Linearization Control of Container Cranes: Varying Rope Length," Int. J. Control Autom. Syst., **5**(4), pp. 379–387.
[20] Tuan, L. A., Lee, S.-G., Dang, V.-H., Moon, S., and Kim, B., 2013, "Partial Feedback Linearization Control of a Three-Dimensional Overhead Crane," Int. J. Control Autom. Syst., **11**(4), pp. 718–727.
[21] Utkin, V., Guldner, J., and Shi, J., 2009, *Sliding Mode Control in Electromechanical Systems*, 2nd ed., Taylor and Francis, London.
[22] Levant, A., 1993, "Sliding Order and Sliding Accuracy in Sliding Mode Control," Int. J. Control, **58**(6), pp. 1247–1263.
[23] Levant, A., 2003, "High-Order Sliding Modes, Differentiation and Output Feedback Control," Int. J. Control, **76**(9), pp. 924–941.
[24] Shtessel, Y., Edwards, C., Fridman, L., and Levant, A., 2014, *Sliding Mode Control and Observation*, Birkhäuser, New York.
[25] Boiko, I., 2009, *Discontinuous Control Systems: Frequency-Domain Analysis and Design*, Birkhäuser, Boston.
[26] Bartolini, G., Pisano, A., and Usai, E., 2002, "Second-Order Sliding-Mode Control of Container Cranes," Automatica, **38**(10), pp. 1783–1790.
[27] Tuan, L., Kim, J.-J., Lee, S.-G., Lim, T.-G., and Nho, L., 2014, "Second-Order Sliding Mode Control of a 3D Overhead Crane With Uncertain System Parameters," Int. J. Precis. Eng. Manuf., **15**(5), pp. 811–819.
[28] Ngo, Q. H., and Hong, K.-S., 2012, "Sliding-Mode Antisway Control of an Offshore Container Crane," IEEE/ASME Trans. Mechatron., **17**(2), pp. 201–209.
[29] Ngo, Q., and Hong, K.-S., 2012, "Adaptive Sliding Mode Control of Container Cranes," IET Control Theory Appl., **6**(5), pp. 662–668.
[30] Chen, W., and Saif, M., 2011, "Actuator Fault Diagnosis for a Class of Nonlinear Systems and Its Application to a Laboratory 3D Crane," Automatica, **47**(7), pp. 1435–1442.
[31] Castaños, F., and Fridman, L., 2006, "Analysis and Design of Integral Sliding Manifolds for Systems With Unmatched Perturbations," IEEE Trans. Autom. Control, **51**(5), pp. 853–858.
[32] Ferreira, A., Punta, E., Fridman, L., Bartolini, G., and Delprat, S., 2014, "Nested Backward Compensation of Unmatched Perturbations Via HOSM Observation," J. Frank. Inst., **351**(5), pp. 2397–2410.
[33] Ferreira, A., Bejarano, F. J., and Fridman, L., 2013, "Unmatched Uncertainties Compensation Based on High-Order Sliding Mode Observation," Int. J. Robust Nonlinear Control, **23**(7), pp. 754–764.
[34] Davila, J., 2013, "Exact Tracking Using Backstepping Control Design and High-Order Sliding Modes," IEEE Trans. Autom. Control, **58**(8), pp. 2077–2081.
[35] Lee, H.-H., 1998, "Modeling and Control of a Three-Dimensional Overhead Crane," ASME J. Dyn. Syst. Meas. Control, **120**(4), pp. 471–476.
[36] Spong, M., 1994, "Partial Feedback Linearization of Underactuated Mechanical Systems," IEEE/RSJ/GI International Conference on Intelligent Robots and Systems, Munich, Sept. 12–16, Vol. 1, pp. 314–321.
[37] Weinmann, A., 1991, *Uncertain Models and Robust Control*, Springer-Verlag, New York.
[38] Utkin, V., 2013, "On Convergence Time and Disturbance Rejection of Super-Twisting Control," IEEE Trans. Autom. Control, **58**(8), pp. 2013–2017.
[39] Polyakov, A., and Poznyak, A., 2009, "Lyapunov Function Design for Finite-Time Convergence Analysis: Twisting Controller for Second-Order Sliding Mode Realization," Automatica, **45**(2), pp. 444–448.
[40] Moreno, J. A., 2012, "A Lyapunov Approach to Output Feedback Control Using Second-Order Sliding Modes," IMA Journal of Math. Control Inf., **29**(3), pp. 291–308.
[41] Polyakov, A., and Fridman, L., 2014, "Stability Notions and Lyapunov Functions for Sliding Mode Systems," J. Frank. Inst., **351**(4), pp. 1831–1865.
[42] Omar, H. M., and Nayfeh, A. H., 2005, "Gantry Crane Gain Scheduling Feedback Control With Friction Compensation," J. Sound Vib., **281**(1–2), pp. 1–20.
[43] Anderson, P. M., and Bose, A., 1983, "Stability Simulation of Wind Turbine Systems," IEEE Trans. Power Appar. Syst., **102**(12), pp. 3791–3795.
[44] Biagiotti, L., and Melchiorri, C., 2008, *Trajectory Planning for Automatic Machines and Robots*, Springer-Verlag, Berlin, p. 194.